

A New Monoclonal Antibody Enables BAR Analysis of Subcellular Importin β Interactomes

Authors

Didi-Andreas Song, Stefanie Alber, Ella Doron-Mandel, Vera Schmid, Christin A. Albus, Orith Leitner, Hedva Hamawi, Juan A. Oses-Prieto, Nili Dezorella, Alma L. Burlingame, Mike Fainzilber, and Ida Rishal

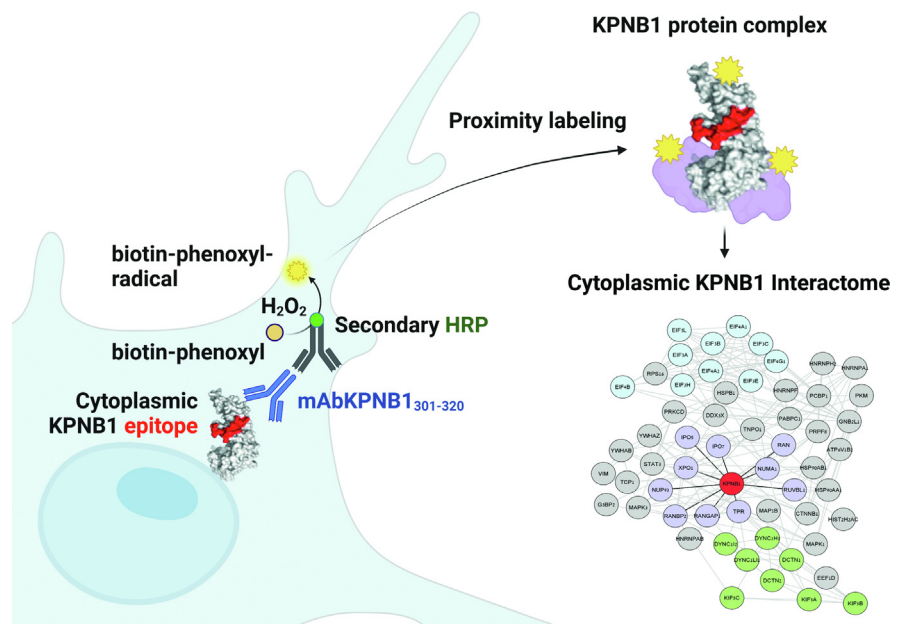
Correspondence

ida.rishal@weizmann.ac.il

Graphical Abstract

In Brief




Proximity biotinylation with a new monoclonal antibody reveals subcellular importin β interactomes.



Highlights

- BioID with KPNB1 has limited efficiency for identifying bona fide importin cargos.
- A new monoclonal antibody targets conserved residues 301-320 in KPNB1.
- The antibody is specific for cytoplasmic Importin β complexes.
- BAR with the novel antibody reveals cytoplasmic importin β interactomes.

A New Monoclonal Antibody Enables BAR Analysis of Subcellular Importin β 1 Interactomes

Didi-Andreas Song^{1,‡}, Stefanie Alber^{1,‡}, Ella Doron-Mandel^{1,‡}, Vera Schmid¹,
Christin A. Albus¹, Orith Leitner², Hedva Hamawi², Juan A. Osés-Prieto³,
Nili Dezarella⁴, Alma L. Burlingame³, Mike Fainzilber¹, and Ida Rishal^{1,*}

Importin β 1 (KPNB1) is a nucleocytoplasmic transport factor with critical roles in both cytoplasmic and nucleocytoplasmic transport, hence there is keen interest in the characterization of its subcellular interactomes. We found limited efficiency of BioID in the detection of importin complex cargos and therefore generated a highly specific and sensitive anti-KPNB1 monoclonal antibody to enable biotinylation by antibody recognition analysis of importin β 1 interactomes. The monoclonal antibody recognizes an epitope comprising residues 301-320 of human KPNB1 and strikingly is highly specific for cytoplasmic KPNB1 in diverse applications, with little reaction with KPNB1 in the nucleus. Biotinylation by antibody recognition with this novel antibody revealed numerous new interactors of importin β 1, expanding the KPNB1 interactome to cytoplasmic and signaling complexes that highlight potential new functions for the importins complex beyond nucleocytoplasmic transport. Data are available via ProteomeXchange with identifier PXD032728.

Transport across the nuclear envelope is an active receptor-mediated process, which is essential for normal cell function (1). The importin β protein family transports cargos with nuclear localization signals (NLS) into the nucleus. Most importin β s bind their cargos directly, while the canonical importin β 1 (also termed karyopherin β 1, KPNB1) uses one of the accessory importin α family members as cargo-binding subunits (2). Ran-regulated association of importin β 1/ α /NLS-cargo complexes in the cytoplasm and their dissociation in the nucleoplasm enables nucleocytoplasmic transport (Fig. 1A). In addition to its key role in nucleocytoplasmic transport, importin β 1 forms cytoplasmic transport complexes with the microtubule motor dynein (Fig. 1B). Importin β 1-dependent cytoplasmic transport has been implicated in long distance signaling in large cells, especially neurons, with roles in injury signaling, size regulation, and growth control (3, 4).

Subcellular localization is an important determinant of biological function, hence there is keen interest in determining importin interactomes and importin-dependent protein partitioning within cells (5). Comprehensive characterization of importin interactomes is challenging due to the transient nature of importin-cargo interactions and the overlapping specificities of different importin complexes. Hence, most previous studies have focused on identifying importin carriers for specific cargo proteins, revealing a diverse range of both direct and indirect KPNB1 interactors (e.g. (6–10)). Other studies have attempted to identify importin cargos from transport perturbation studies (11, 12) or from transcriptome analyses after genetic perturbations (e.g. (13–16)). Unbiased proteome-wide studies have used proximity biotinylation to characterize an importin β 1 interactome in human embryonic kidney (HEK) cells (17) and affinity proteomics to identify interactors in mitotic cells (18, 19). These diverse studies have unveiled an expanding list of KPNB1 interactors but for the most part do not shed light on subcellular specializations in importin β 1 interactions.

As noted above, importin β 1 has specific cytoplasmic roles in cell size sensing and in neuronal injury signaling that are distinct from its nucleocytoplasmic transport activity (20–23). We therefore sought methods for comprehensive subcellular studies of its interactomes. A diverse range of proximity-based biotinylation assays provide powerful tools to label and subsequently detect interacting proteins (24). Initial tests of BioID (25) suggested limited efficiency of the method for both N- and C-terminal fusions of KPNB1 with the modified biotin ligase BirA. We therefore generated a monoclonal antibody (mAb) to enable biotinylation by antibody recognition (BAR) (26, 27), which is based on antibody-guided deposition of a horseradish peroxidase (HRP) enzyme to generate tyramide (phenoxy) radicals (28, 29). The antibody targets a 20 amino acid epitope that is highly conserved in mammalian

From the ¹Departments of Biomolecular Sciences and Molecular Neuroscience, and ²Life Science Core Facilities, Faculty of Biochemistry, Weizmann Institute of Science, Rehovot, Israel; ³Department of Pharmaceutical Chemistry, University of California, San Francisco, California, USA; ⁴Electron Microscopy Unit, Department of Chemical Research Support, Weizmann Institute of Science, Rehovot, Israel

[‡]These authors contributed equally to this work.

*For correspondence: Ida Rishal, ida.rishal@weizmann.ac.il.

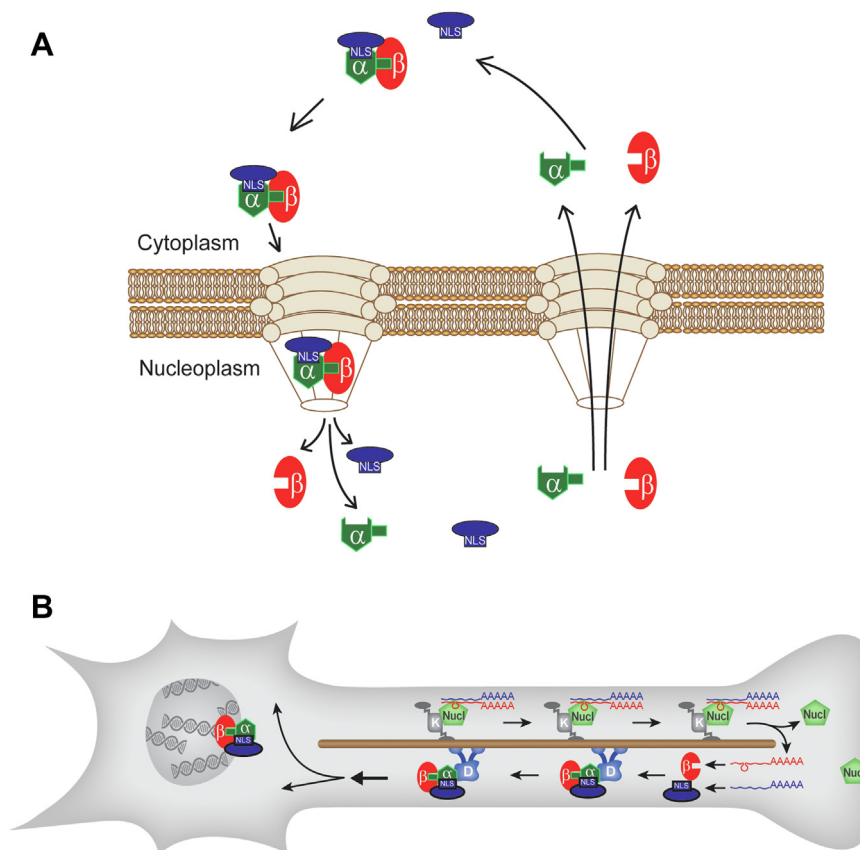


FIG. 1. **Importin β 1 roles in intracellular transport.** A, nucleocytoplasmic transport by importin β 1 in complex with an importin α traffics NLS-bearing cargos through the nuclear pore complex (NPC). B, importin β 1-mediated transport in neuronal cytoplasm occurs upon local translation of anterogradely transported importin β 1 mRNA, followed by formation of a retrogradely transported importins-cargo complex. α , importin α ; β , importin β 1; D, dynein; K, kinesin; Nucl, nucleolin; NLS, nuclear localization signal.

KPNB1 and discriminates between nuclear and cytoplasmic protein complexes, allowing rigorous characterization of cytoplasmic importin β 1 interactomes using the BAR method.

EXPERIMENTAL PROCEDURES

Animals

All animal procedures were performed in accordance with the guidelines approved by the Weizmann Institute of Science Institutional Animal Care and Use Committee. Animals were purchased from Envigo Ltd (Israel) or originate from in-house breeding. Female BALB/c mice (6–8 weeks, Envigo) were used for immunization and subsequent isolation of spleen cells. Follow-up antibody characterization experiments were performed on male C57BL6 mice (8–12 weeks, Envigo) and as well as male Wistar rats (8–12 weeks, Envigo). All animals were maintained at the Veterinary Resources department of the Weizmann Institute with free access to food and water.

Sciatic Nerve Crush

Animals were anesthetized with ketamine/xylazine (10 mg/kg of body weight intraperitoneal). Sciatic nerve (SN) crush was performed at the mid-thigh level using fine jeweler forceps in two adjacent positions for 30 s each. Only one side was subjected to crush injury, the contralateral side served as an uninjured control. SNs were

excised 6 and 24 h after injury, fixed and processed for immunohistochemistry.

Reagents and Antibodies

Commercially available primary antibodies used in this study for immunoprecipitation (IP), immunofluorescence (IF), proximity ligation assay (PLA), Western blot (WB), and Simple Western capillary system (WES) were as follows: anti-GFP (abcam, ab6556, IF & WB 1:5000, PLA 1:2000), anti-NFH (abcam, ab72996, 1:2000), anti-Actin (MP, clone C4, 08691001, WB 1:5000), anti-GAPDH (Santa Cruz Biotechnology, sc-32233, WB 1:5000), anti-ERK1/2 (Sigma, M5670, WB 1:30000), anti- β -III tubulin TUJ1 (abcam, ab18207, IF 1:1000, WB: 1:6000), anti-Dynein heavy chain (DYNC1H1, Proteintech, #12345-1-AP, PLA 1:50), anti-importin beta 1 (MBS713065, rabbit, polyclonal, 1:1000), and rabbit anti-nucleolin (ProteinTech, 10556-1-AP, 1:100 for IF).

Plasmids and Constructs

Expression constructs for KPNB1 were based on pEGFP-N1 human full-length KPNB1 from Addgene (#106941). The KPNB1 coding DNA sequence was amplified from pEGFP-N1 human full-length KPNB1 (Addgene #106941) and mVenus coding DNA sequence was amplified from pTrix-mVenus-PA-Rac1 (Addgene #22007). For seamless protein engineering of importin β 1 BioID constructs, all cloning steps were carried out using restriction-free cloning following published protocols

(30, 31). All primers were designed such that the protein domains (BirA*, ImpB1, and mVenus) are separated by a small flexible GS-dipeptide. Briefly, the multiple cloning site of pcDNA3.1 mycBioID (Addgene #35700) was removed to generate the Myc-BirA* control. Subsequently, the KPNB1 coding sequence was inserted either downstream or upstream of BirA* to generate N- or C-terminally BirA*-tagged importin β 1 fusion constructs, respectively. The opposite terminus of importin β 1 was fused to mVenus (amplified from pTrix-mVenus-PA-Rac1, Addgene #22007) which has a similar size to BirA* to ensure similar molecular behavior of both fusion constructs. Detailed cloning procedure is described in the [Supplementary Data](#).

Generation of Monoclonal Antibodies

The antibody was raised against full-length recombinant mouse importin β 1 protein (UniProt accession # P70168) with an N-terminal His-tag produced in yeast (MyBioSource: cat # MBS955236). Importin β 1 protein was dissolved in 1xPBS and mixed with Complete Freund's Adjuvant (CFA) in a double-glass syringe at a volume ratio of 1:1 (23 μ g protein in 50 μ l 1xPBS +50 μ l CFA/mouse) for immunization. Five BALB/c female mice (6–8 weeks old) were used for immunization by footpad injection into both hindlimbs (50 μ l/food pad). Two weeks later, mice were boosted with the same dose (boost 1: 23 μ g protein in 100 μ l/mouse) intradermally in several spots in the belly area and limbs (close to lymph nodes). Retroorbital bleeding was performed 1 week later and serum was tested by ELISA to determine the mouse with the highest immune response. Four weeks after boost 1, the mouse with the highest immune response received a pre-fusion boost (IP injection of 20 μ g protein in 200 μ l 1xPBS, without CFA) and was sacrificed 4 days later to collect immune cells from the spleen. Approximately, 100 million spleen cells were harvested and collected in Dulbecco's modified Eagle's medium (DMEM) for the production of hybridoma cell lines. The timeline of the immunization procedure is shown in [supplemental Fig. S2A](#).

Hybridomas were generated as previously described (32). BALB/c female mouse splenocytes were fused with NS0 nonsecreting murine myeloma cells using 41% PEG in DMEM (Roth). Hybrid cells were selected in growth medium supplemented with HAT (hypoxanthine, aminopterin, and thymidine) (100 \times HAT media supplement, Sigma-Aldrich). Culture supernatants from wells with viable clones were screened by an indirect ELISA using recombinant importin β 1 protein. Stable hybridoma clones secreting importin β 1 specific antibodies were obtained after two cloning cycles by a limiting dilution assay and were weaned from HAT supplements. Hybridoma cells were grown in complete DMEM (Biochrom) supplemented with 15% fetal bovine serum (FBS, Biochrom), 2 mM L-glutamine, 10,000 units penicillin, 10,000 units streptomycin, 1 mM Na pyruvate, with or without HAT supplements (1:100 from stock). The final positive hybridoma cells secreting antibodies against importin β 1 were stored in liquid nitrogen. All procedures involving experimental mice were performed under controlled laboratory conditions in strict accordance with Institutional Animal Care and Use Committee guidelines. A schematic of the selection process and hybridoma propagation is shown in [supplemental Fig. S2B](#). For more detailed protocols, see [Supplementary Material](#).

Enzyme-Linked Immunosorbent Assay

Indirect ELISA was performed in 96-well plates (NUNC-442404), coated with full-length importin β 1 protein (1 μ g/ml in 1xPBS) overnight at 4 $^{\circ}$ C, and then blocked by incubation with 10 mg/ml bovine serum albumin (BSA) in 1xPBS for 1 h at RT. Hybridoma supernatant or purified and diluted Abs were applied and incubated for 1 h at RT, followed by HRP-conjugated anti-mouse Fab fragments (1 h RT, 1:60,000) as the secondary antibody (Sigma A9917-1 ml). HRP substrate (TMB Sigma T0565-100 ml) was added subsequently and the absorbance was recorded at 630 nm using a microplate reader

(Thermo Fisher Scientific). In between steps, plates were washed in PBST (PBS containing 0.05% Tween-20) three times. For linear ELISA, coating was done with a serial dilution of the full-length importin β 1 protein (0.001, 0.01, 0.1, 1 μ g/ml), to explore the linear range of antibody-antigen recognition.

Antibody Isotyping & Purification

Immunoglobulin isotyping test was performed using a mouse mAb isotyping kit, according to the manufacturer's instructions (SBA Clo-ntotyping System-HRP, SouthernBiotech, 5300-05). Monoclonal antibodies were purified by Protein A affinity purification, using an AKTA PURE system. The purified fraction was desalted in 1XPBS, using a HiPrep desalting column and stored at 2 to 8 $^{\circ}$ C.

DRG Culture

Adult mouse dorsal root ganglia (DRG) neuron culture was performed as previously described (33). Briefly, the ganglia were dissociated with 100 U of papain (P4762, Sigma) followed by 1 mg/ml collagenase-II (11179179001, Roche) and 1.2 mg/ml dispase-II (04942078001, Roche). The DRGs were triturated in 1xHBSS, 10 mM glucose, and 5 mM Hepes (pH 7.35) using a fire-coated Pasteur pipette and then layered on 20% percoll in L15 media and recovered by centrifugation at 1000g for 8 min. Cells were washed briefly in growth media (F12, 10% FBS, Primocin (100 μ g/ml, InvivoGen #ant-pm-1)) and plated on poly-L-lysine (P4832, Sigma) and laminin (23017-015, Invitrogen)-coated glass coverslips. Culture media and serum were purchased from Thermo Fisher Scientific. DRG neurons were grown for 24 to 48 h in culture at 37 $^{\circ}$ C and 5% CO₂.

Cell Line Cultures

HeLa cells (human, female, RRID: CVCL_0030), HEK-293 (human, female, RRID: CVCL_0045), NIH/3T3 (mouse, male, RRID: CVCL_0594), and Neuro-2A (mouse, male, RRID: CVCL_0470) cells were purchased from ATCC (Cat# CCL-2, CRL-1573, CRL-1658, CCL-131, respectively). All cell lines were cultured in DMEM (Gibco), supplemented with 10% FBS (Gibco), 100 U/ml penicillin, and 100 μ g/ml streptomycin. All cells were incubated at 37 $^{\circ}$ C and 5% CO₂.

Protein Extraction for SDS Page, Western Blot, and WES

For total protein extraction, tissues were collected in RIPA buffer (150 mM NaCl, 1.0% NP-40, 0.5% sodium deoxycholate, 0.1% SDS, 50 mM Tris, pH 8.0.), supplemented with protease/phosphatase/RNase inhibitors (complete protease inhibitor EDTA-free (Roche 1187358000), phosphatase inhibitor cocktail 2 (1/1000, Sigma 5726), phosphatase inhibitor cocktail 3 (1/1000, Sigma P0044), and RNase inhibitor (200 U/ml, RNAsen, Promega N251B)). Tissue samples were homogenized in Dounce Tissue Grinders (WHEATON 33, 1 ml #357538, 7 ml #357542) or, using plastic pestles, in an Eppendorf tube.

The axoplasm for biochemical analysis was extracted from mouse, rat, or bovine SN as previously described (34). To minimize glia contamination, transport buffer (TB) was used in this extraction protocol (20 mM Hepes, 110 mM KAc, 5 mM MgAc, pH 7.4 supplemented with protease/phosphatase/RNase inhibitors). All protein extracts were incubated on ice for 20 min, followed by a spin at 10,000g for 10 min at 4 $^{\circ}$ C.

For WB, proteins were blotted on nitrocellulose membranes using a Trans-Blot Turbo Transfer System (Bio-Rad). Membranes were blocked with 5% nonfat dry milk in 1xTBST buffer for 1 h. Primary antibodies were incubated for 1 h at room temperature or overnight at 4 $^{\circ}$ C with shaking. Secondary HRP-conjugated antibodies were diluted 1:10,000 in 1xTBST and incubated for 1 h at room temperature. Blots were developed using Radiance ECL substrate (Azure

biosystems) or SuperSignal West Femto (Thermo Fisher Scientific) substrates on an Amersham Imager 680. Automated capillary electrophoresis immuno-quantification runs were conducted on a WES instrument (ProteinSimple) as described (35). The indicated molecular weights are based on an internal standard spiked into every capillary.

Proximity Ligation Assay

PLA was performed on cultured DRG neurons using the Duolink system (Sigma) according to the manufacturer's instructions with minor modifications. DRG neurons (isolated from C57BL6 mice) were fixed in 4% paraformaldehyde (PFA) after 48 h in culture. Blocking was performed in 5% donkey serum with 1% BSA in 1xPBS for 30 min, followed by primary antibody incubation for 1 h at room temperature. Combinations: rabbit anti-DYNC1H1 (Proteintech, #12345-1-AP, 1:50) or rabbit anti-importin β 1 (MBS713065, 1:1000), together with the antibody generated in the present study mouse anti-importin β 1 (mAbKPNB1-301-320, 1 μ g/ml). As controls, each antibody was used by itself, and furthermore, we used mAbKPNB1-301-320 in combination with another rabbit antibody (GFP, abcam, ab6556, 1:2000). Interactions (PLA signals) were detected using Sigma PLA probe anti-mouse minus DUO92004, anti-rabbit plus DUO92002, and detection kits Red DUO92008 or FarRed DUO92013 according to the manufacturer's instructions and incubation times. The PLA protocol was followed by IF staining for neurofilament heavy chain (abcam, ab72996, 1:2000, 45 min at RT) with Alexa 488 donkey anti-chicken secondary antibody (45 min at RT). The quantification of the PLA signal was performed on neurofilament heavy chain-positive axons using Fiji (36).

Electron Microscopy

DRG neurons were grown on 3-mm carbon-coated Sapphire disks (Wohlwend GmbH) and fixed 48 h after plating by high-pressure freezing using a Leica EM ICE (Leica Microsystems GmbH), followed by freeze substitution in a temperature-controlled device, AFS2 (Leica Microsystems GmbH), washing, embedding in Lowicryl HM20, and ultrathin sectioning (70–90 nm). Sections were collected on nickel grids. For immunostaining, grids were washed, incubated for 30 min in blocking solution (0.5% gelatin, 0.5% BSA, 0.2% glycine, 3% NGS in PBS), and then incubated for 2 h in mAbKPNB1-301-320 (1 mg/ml stock, dilutions: 1:10, 1:100) with or without blocking peptide KPNB1₃₀₁₋₃₂₀, with a ratio of 4.6 nM mAbKPNB1-301-320 to 9.5 nM peptide. After washing with PBS containing 0.2% glycine, the sections were incubated for 15 min in blocking solution and then for 30 min in 10-nm colloidal-gold-conjugated goat anti mouse antibodies (Electron Microscopy Sciences) (1:20), followed by sequential washing in PBS containing 0.2% glycine and in bi-distilled water. The grids were then stained with Reynolds lead citrate and analyzed under 120 kV on a Thermo Fisher Scientific Tecnai T12 transmission electron microscope equipped with a bottom mounted TVIPS TemCam-XF416 4k \times 4k CMOS camera using TVIPS EMplified software (<https://www.tvips.com/imaging-software/em-menu/>).

Pull-Down From Rat Brain

Whole brain was isolated from adult Wistar rats (male, 8–12 weeks, Envigo) and homogenized in 7 ml Dounce Tissue Grinders (WHEATON 33, 7 ml #357542) in transport buffer, supplemented with NP-40 (20 mM Hepes, 110 mM KAc, 5 mM MgAc, pH 7.4 supplemented with complete protease inhibitor, phosphatase inhibitor cocktail 2 & 3, as well as 0.5% NP-40 for the initial lysis, then for the IP diluted to 0.035%). For each IP sample, 1 mg of total brain extract was used and adjusted with TB to a total volume of 300 μ l and a final concentration of 0.035% NP-40. 10% (30 μ l) was taken as input. The remaining lysate for the IP was incubated for 3 h at 4 $^{\circ}$ C with overhead rotation with 10 μ g of mAbKPNB1-301-320 or control (preblocked

mAbKPNB1-301-320: 10 μ g Ab with 50 μ g blocking peptide (KPNB1₃₀₁₋₃₂₀) for 1 h). Subsequently, 100 μ l Protein G magnetic beads (Dynabeads, Thermo Fisher Scientific 10004D), preblocked with salmon sperm DNA (10 μ l DNA per 100 μ l beads for 1 h 4 $^{\circ}$ C), were added to the brain lysate-Ab mixture and incubated for additional 2 h at 4 $^{\circ}$ C. Beads were washed in several steps with different buffers as follows: TB-0.1% NP-40 for 3 min, TB-0.5% NP-40 3 min, TB-1% NP-40 1 min, TB- no detergent 3 min. For simple Western blotting, elution from beads was conducted by denaturing the proteins from the beads with WES sample buffer supplemented with DTT to a final concentration of 40 mM for 5 min at 95 $^{\circ}$ C.

BioID in HeLa Cells

HeLa cells were transfected using jetPEI (Polyplus-transfectionSA) according to the manufacturer's protocol and supplemented with 50 μ M Biotin (Molecular Probes) for 24 h. Cells were grown on 10 cm plates for mass spectrometry analyses. For streptavidin-IP from whole cell lysates, cells were lysed with 1.5 ml/plate lysis buffer (50 mM Tris HCl, pH 7.5, 150 mM NaCl, 0.25% (w/v) NP-40, 1 mM MgCl₂, 5 mM KCl, 2.5 mM EDTA, 1% (w/v) Triton X-100, 0.1% (w/v) SDS, 1 mM DTT, 1 \times Complete protease inhibitor, EDTA-free (Roche)), sonicated (30% amplitude, ten cycles of 5.5 s pulse on, 9.9 s pulse off), and lysates from six plates were incubated with 600 μ l streptavidin beads for 4 h. Beads (Dynabeads MyOne streptavidin C1, Thermo Fisher Scientific) were then washed twice with wash buffer I (2% (w/v) SDS), once with wash buffer II (0.1% (w/v) deoxycholic acid, 1% (w/v) Triton X-100, 1 mM EDTA, 500 mM NaCl, 50 mM Tris HCl, pH 7.5), once with wash buffer III (0.5% (w/v) deoxycholic acid, 0.5% (w/v) NP-40, 1 mM EDTA, 250 mM LiCl, 10 mM Tris HCl, pH 7.5), twice with 50 mM Tris HCl, pH 7.5, and once with (20 mM Tris HCl pH 8.0, 2 mM CaCl₂) (37) prior to processing for mass spectrometry.

BAR Assays in HEK Cells and DRG Neurons

HEK 293T cells were grown in DMEM high glucose 5 g/l (Sigma-Aldrich) supplemented with 10% heat inactivated FBS. Cells were seeded at a density of 1.2e4 cells/cm² and monitored over 24 h until reaching 70% confluency. Cells were then fixed in 4% PFA and permeabilized with Triton X-100 for 10 min at RT, subsequently, incubated for 3 h at 4 $^{\circ}$ C with blocking solution. 2.7 μ g/ml mAbKPNB1-301-320 was added in blocking buffer and incubated overnight at 4 $^{\circ}$ C. The next day, cells were washed three times with 1xPBST and incubated with secondary HRP-conjugated antibody for 3 h at 4 $^{\circ}$ C prior to tyramide signal amplification according to the manufacturer's protocol. Cells were harvested and boiled for 1 h at 99 $^{\circ}$ C for reverse cross-linking followed by streptavidin beads affinity purification and processing for proteolytic digest and mass spectrometry.

Adult DRG neuronal cultures were prepared as previously described (33). The culture was maintained for 72 h with daily supplement of glia inhibitor AraC (10 μ M). The cells were then fixed in 4% PFA for 20 min at room temperature followed by three washes with 1xPBST, permeabilization with 0.1% Triton X-100, and incubation in blocking solution for 3 h at 4 $^{\circ}$ C. 2.7 μ g/ml mAbKPNB1-301-320 was added in blocking buffer and incubated overnight at 4 $^{\circ}$ C. The next day, cells were washed three times with 1xPBST and incubated with secondary HRP-conjugated antibody for 3 h at 4 $^{\circ}$ C. The tyramide signal amplification was performed according to the manufacturer's protocol (Tyramide SuperBoost Kits with Alexa Fluor Tyramides, Invitrogen). The cells were then harvested and boiled for 1 h at 99 $^{\circ}$ C for reverse crosslinking followed by purification of the streptavidin beads affinity before processing for mass spectrometry.

Mass Spectrometry Analysis for BioID Assay Samples

Sample-incubated streptavidin magnetic beads were resuspended in 20 μ l 5 mM DTT, 100 mM NH₄HCO₃ and incubated for 30 min at

room temperature. Subsequently, iodoacetamide was added to a final concentration of 7.5 mM and the samples were incubated for 30 additional minutes. 0.5 μ g of sequencing grade trypsin (Promega) was added to each sample and incubated at 37 °C overnight. Supernatants of the beads were recovered, and beads were digested again using 0.5 μ g trypsin in 100 mM NH_4HCO_3 for 2 h. Peptides from both consecutive digestions were combined and recovered by solid phase extraction using C18 ZipTips (Millipore), eluted in 15 μ l 50% acetonitrile, 0.1% formic acid, and resuspended in 5 μ l 0.1% formic acid for analysis by LC-MS/MS.

Peptides resulting from trypsinization were analyzed on a QExactive Plus (Thermo Scientific), connected to a NanoAcquity Ultra Performance UPLC system (Waters). A 15-cm EasySpray C18 column (Thermo Scientific) was used to resolve peptides (90-min 2–30% gradient with 0.1% formic acid in water as mobile phase A and 0.1% formic acid in acetonitrile as mobile phase B). Mass spectrometer was operated in positive ion mode and in data-dependent mode to automatically switch between MS and MS/MS. MS spectra were acquired between 350 and 1500 m/z with a resolution of 70,000. The top 10 precursor ions with a charge state of 2+ or higher over the selected threshold (1.7E4) were fragmented by higher-energy dcollisional dissociation using a normalized collision energy of 25 with an isolation window of 4 m/z. MS/MS spectra were acquired in centroid mode with resolution of 17,500 from m/z = 100. A dynamic exclusion window was applied which prevented the same m/z from being selected for 10 s after its acquisition.

For peptide and protein identification, peak lists were generated using PAVA in-house software (38). All generated peak lists were searched against the human subset of the SwissProt.2019.07.31 database (containing 20,432 entries) using Protein Prospector (39) with the following parameters: enzyme specificity was set as Trypsin, and up to two missed cleavages per peptide were allowed. Carbamidomethylation of cysteine residues was allowed as fixed modification. N-acetylation of the N-terminus of the protein, loss of protein N-terminal methionine, pyroglutamate formation from peptide N-terminal glutamines, and oxidation of methionine were allowed as variable modifications. Mass tolerance was 10 ppm in MS and 30 ppm in MS/MS. The false positive rate was estimated by searching the data using a concatenated database which contains the original SwissProt database, as well as a version of each original entry where the sequence has been randomized. A 1% false discovery rate was permitted at the protein and peptide level. All spectra identified as matches to peptides of a given protein (Peptide Spectral Matches, PSMs) were reported, and this number is used for label-free quantitation of relative protein abundances in the samples as ratios of each protein PSMs to the average PSMs for that protein on the appropriate control samples (cells transfected with Myc-BirA). Absent values were given a PSM value of 0.5.

Mass Spectrometry Analysis of BAR Assay Samples

On-bead digestion was performed as indicated above. Peptides resulting from trypsinization were analyzed on an Orbitrap Lumos Fusion (Thermo Scientific), connected to a NanoAcquity Ultra Performance UPLC system (Waters). A 15-cm EasySpray C18 column (Thermo Scientific) was used to separate peptides in a 60-min 2 to 30% gradient with 0.1% formic acid in water as mobile phase A and 0.1% formic acid in acetonitrile as mobile phase B. MS was operated in positive ion mode and in data-dependent mode to automatically switch between MS and MS/MS. MS spectra were acquired between 375 and 1500 m/z with a resolution of 120,000. For each MS spectrum, multiple charged ions over the selected threshold (2e4) were selected for MS/MS in cycles of 3 s, with an isolation window of 1.6 Th. Precursor ions were fragmented by higher-energy dcollisional dissociation using a normalized collision energy of 30. MS/MS spectra were acquired in centroid mode with resolution 30,000 from m/z = 110. A dynamic exclusion

window was applied which prevented the same m/z from being selected for 30 s after its acquisition. MS data analysis was performed as indicated for BioID samples above, but in the case of data from DRG mouse neurons, the mouse subset (17,009 entries) of the SwissProt.2019.07.31 database was used to search the data.

Experimental Design and Statistical Rationale

BioID and DRG BAR experiments were performed in three biological replicates, while BAR on HEK cells was in duplicates. Control samples used in BioID were Myc-BirA* and samples omitting mAbKPNB1-301-320 for BAR experiments. Proteins whose corresponding peptides count was less than two in all replicates were excluded from the analysis in BioID experiments. Proteins whose corresponding peptides were not found in all replicates as well as keratin contaminants were excluded from the analysis in BAR experiments. To assess the statistical significance of protein fold changes between treatment conditions, log₂ fold change ratios were averaged across replicates and *p*-values were calculated using *Prism* software (GraphPad) applying multiple unpaired *t* test (two-stage step-up Benjamini, Krieger, and Yekutieli (40)) with a desired false discovery rate of 10%.

Immunofluorescence and Immunohistochemistry on Cryosections

Sensory neurons were grown on glass coverslips coated with Poly-L-lysine and Laminin for 2 days and then fixed using 4% PFA, permeabilized with 0.2% Triton X for 10 min at 25 °C, and blocked for 1 h at room temperature with 5% BSA in 1XPBST. Coverslips with neurons were incubated in mAbKPNB1-301-320 with or without blocking peptide KPNB1₃₀₁₋₃₂₀, with a ratio of 4.6 nM mAbKPNB1-301-320 to 9.5 nM peptide, overnight at 4 °C. After three five-minute washes in 1xPBS, cells were incubated in donkey anti-mouse FITC secondary antibodies (1:200 each; Jackson Immuno-Res) for 1 h at room temperature. After three 5 min washes in 1xPBS, coverslips were rinsed in ddH₂O, then mounted with Prolong Gold Antifade with DAPI.

SNs of adult WT mice were dissected at the designated times after crush injury and noninjured controls, fixed in 4% PFA for 12 h at 4 °C. Then nerves were washed three times in 1XPBST (10 min each), incubated overnight in 30% sucrose and subsequently embedded in OCT freezing medium. The 12 μ m thick sections were cut with a cryostat and mounted on glass slides. Freshly cut sections were incubated in blocking solution (5% BSA in 1XPBST) for 2 h at 4 °C and incubated overnight with primary antibody (in 1XPBST with 2% BSA). Primary antibody solution was carefully removed and slides were washed three times (5 min each) at room temperature with 1XPBST. In the next step, the slides were incubated in donkey anti-mouse FITC secondary antibodies (1:1000 each; Jackson Immuno-Res) for 2 h at room temperature. After three 5-min washes in 1XPBST, slides were mounted with Prolong Gold Antifade.

Acquisition and Image Analysis

All fluorescent images including PLA were collected using an Olympus FV1000 Confocal laser-scanning microscope at 60 \times magnification with oil-immersion objective (Olympus UPLSAPO, NA 1.35) or using Fluoview (FV10i), a fully automated confocal laser-scanning microscope, with water immersion objective (Olympus UPLANSAP0 60X, NA 1.2). Image analysis was performed using Fiji software (36) (<https://imagej.net/software/fiji/>).

siRNA Knockdown

N2A cells were seeded in six-well plates with 120,000 cells per well, one day before siRNA transfection. The cells were transfected with custom siRNA against the 3' UTR of mouse importin β 1 (siKPNB1) or siControl #5, using DharmaFECT 4 transfection reagent (Dharmacon) according to the manufacturer's protocol. Forty eight hours after

transfection, the cell growth medium was replaced by serum-free medium to slow down proliferation and to activate the differentiation process. Seventy two hours after transfection, the cells were harvested and total protein was extracted in RIPA buffer containing 0.1% SDS and protease inhibitors. Twenty micrograms of total protein per each sample were run on gel for WB analysis.

Statistical Methods

Data represent mean \pm SEM, unless otherwise noted. Groupwise analyses were conducted by one- or two-way ANOVA with post hoc tests as described in the figure legends. Pairwise analyses were conducted by two-tailed Student's *t* tests (unpaired, unless otherwise noted; see Figure Legends). Statistical analyses were conducted using GraphPad Prism, Synergy Kaleidagraph, or Microsoft Excel. Statistically significant *p* values are shown as **p* < 0.05, ***p* < 0.01, ****p* < 0.001 and *****p* < 0.0001. Physical subnetwork analysis was performed using String database version 11.5 (41). An interaction score of 0.4 was selected and the confidence was based on all available active interaction sources.

Gene ontology analysis was done using metaspape (42) to identify all statistically enriched terms, with a *p* value cut-off of 0.01 and min enrichment of 1.5. The significant terms were hierarchically clustered into a tree diagram, based on Kappa-statistical similarities among their gene memberships. A 0.3 kappa score was applied for term clustering. A selected subset of representative terms from this cluster was converted into a network layout, with each term represented by a circle node and its cluster identity shown in color. Terms with a similarity score >0.3 are linked by an edge (the thickness of the edge represents the similarity score). The network was visualized with Cytoscape (v3.1.2) with a 'force-directed' layout and with edge bundled for clarity.

RESULTS

BioID Proximity Labeling of Importin β 1 Interactors in HeLa Cells

We first tested BioID for proximity labeling of importin β 1 interactomes. The effective labeling range of this method has been estimated as ~10 nm (43), hence fusions of BirA* at the N-terminus of importin β 1 might not label NLS-containing cargos that bind the complex via importin α (Fig. 2, A and B). We therefore generated constructs with BirA* fused to either N- or C-terminus of the human importin β 1 ORF, with a Myc epitope tag and Venus fluorescent protein at the opposite termini (Fig. 2B). These and a control construct comprising only Myc-tagged BirA* were expressed in HeLa cells and expression was validated with either Myc or anti-importin β 1 antibodies. Cells were pulsed with biotin for 24 h, and cell lysates were subjected to streptavidin pull-downs for mass spectrometric analyses. A total of 223 specific hits were identified (supplemental Table S1), of which 54 hits, primarily nuclear pore complex proteins, were shared by both constructs (Fig. 2, C–E and supplemental Fig. S1). Additional candidates include proteins involved in cell division/spindle assembly, RNA splicing, mRNA metabolism and export from the nucleus, and proteins that participate in nuclear import (supplemental Fig. S1). However, importin α 's were identified only with the C-terminal BirA* construct, and the dataset lacked many classical NLS-dependent importin cargos that are known to be expressed in HeLa cells.

In order to determine if NLS-dependent cargos can be efficiently biotin tagged by regular BioID, we designed NLS test constructs featuring either the bipartite NLS of Nucleoplasmin (NLS1) or the monopartite SV40 NLS (NLS2) fused to either the C- or N-terminus of mCherry carrying a FLAG epitope (supplemental Table S2). We cotransfected HeLa cells with these constructs with the Venus-Importin β 1-BirA* construct and incubated with biotin for 24 h. The importin- β -binding domain (IBB) of Importin α fused to mCherry (IBB-mCherry-FLAG) construct was used as a positive control and a FLAG-mCherry construct as a negative control. Robust expression and nuclear localization of IBB-mCherry and all NLS-mCherry fusions were validated by imaging. To test whether these constructs are biotinylated, cells were lysed, biotinylated proteins were captured by streptavidin pull-down, and eluates were probed with anti-FLAG antibody. The IBB-mCherry-FLAG was biotinylated as expected, but neither of the NLS-mCherry test constructs were labeled (data not shown). Since this might be due to the limited biotinylation range of BirA* (43), we generated a series of constructs incorporating linkers of different lengths and flexibility between BirA* and importin β 1 to bring the BirA* enzyme closer to the cargo (supplemental Table S2). These new BioID constructs were cotransfected with NLS1-mCherry-FLAG, and biotinylation of the NLS construct was tested by Streptavidin pull-down and probing of eluates with anti-FLAG antibody. Strikingly, none of the constructs were able to biotinylate the NLS-mCherry-FLAG test construct, whereas the positive control (IBB-mCherry-FLAG) cotransfected with the mVenus-Importin β 1-BirA* construct underwent robust biotinylation (data not shown). This strongly suggests that steric hindrance and limited range may restrict the efficiency of importin β 1-targeted BioID for tagging of endogenous importin cargos.

Tagging an Importin α for BioID instead of importin β 1 is not straightforward, since both the N- and C-termini of Importin α are essential for its functions (44–46). BAR enables proximity labeling of interactors of a protein of interest upon antibody binding (26) and moreover has an effective radius of up to ~0.5 to 1 μ m (47, 48), which might be advantageous for importin interactome characterization. However, the approach is critically dependent on antibody specificity and sensitivity (26). We therefore set out to generate a high-quality mAb for importin β 1.

Antibody Generation and Epitope Mapping

Full-length recombinant mouse importin β 1 protein was used to immunize mice for mAb production. A conventional immunization protocol was conducted on five animals, and the highest responding mouse was selected after verification of serum titer and specificity (supplemental Figs. S2 and S3). The selected mouse underwent a prefusion boost four days prior to spleen cells collection and hybridoma fusion using standard procedures (32). Cell culture supernatants from ~960 hybridoma clones were screened for secretion of anti-importin

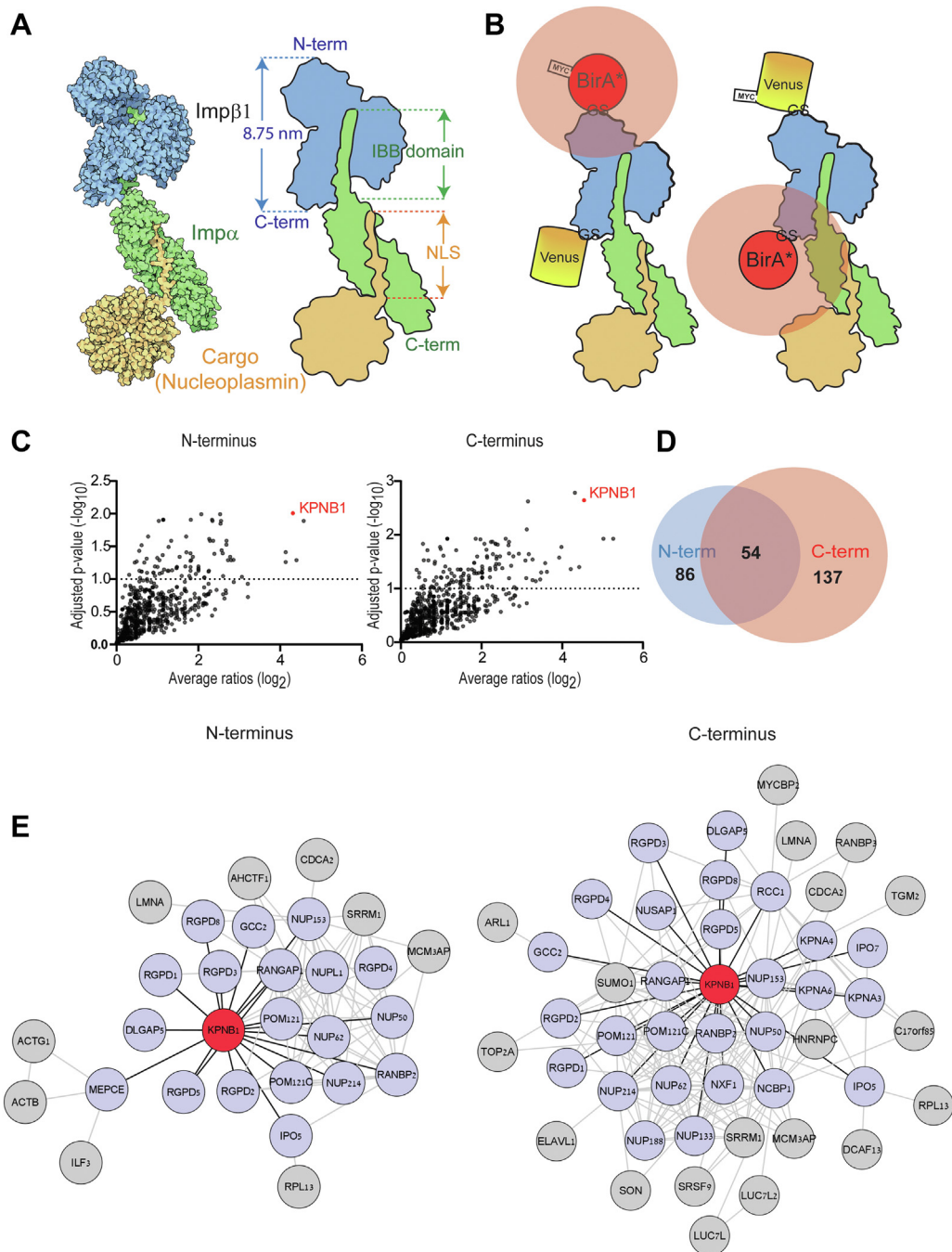


FIG. 2. Importin β 1 BioID. *A*, structural model of the importins complex with an NLS-bearing cargo protein, nucleoplasmin, from <https://pdb101.rcsb.org/motm/85>. *B*, schematic showing a set of KPNB1-BioID constructs superimposed on the structural model. Constructs have N- or C-terminal BirA* fusions and Venus reporter with Myc tag on the opposing termini. Pink shading around BirA* indicates 10 nm range of biotinylation. *C*, volcano plots of label-free LC-MS/MS analysis from HeLa cells overexpressing N- or C-terminal BirA* KPNB1 constructs. *D*, Venn diagram: numbers of significant hits obtained by each construct. *E*, physical network representation of N- and C-terminal KPNB1-BioID interactomes, based on STRING with a cut-off interaction score of 0.4. KPNB1 is highlighted in red, direct interacting partners in light purple, and second order interactors in gray. IBB, importin β 1-binding domain of importin α ; GS, Glycine-Serine linker; NLS, nuclear localization signal.

β 1 antibodies, yielding 20 positive clones. Further screening of these 20 clones included WB for endogenous KPNB1 in bovine axoplasm (supplemental Fig. S3C), IF in different cell

types (HeLa, 3T3, mouse DRG, supplemental Fig. S3D), and ELISA, using linear dilution series (supplemental Fig. S3E). Clones were scored on a scale from 0 (no signal) to 3 (highest

signal) in all applications and the top eight clones underwent subcloning, antibody purification, and isotyping (supplemental Fig. S3F). Purified antibody from these eight clones were validated again by ELISA (supplemental Fig. S3G). All these eight antibodies were able to detect importin β 1, with some mainly showing nuclear signal, while others revealed a clear preference for cytoplasmic importin β 1. The antibody with the highest overall score from those with preferential immunoreactivity for cytoplasmic importin β 1 was chosen for further characterization.

We used a custom peptide library screen to identify the epitope recognized by the selected mAb. Fifty eight overlapping peptides with a length of 20 amino acids (aa) each were synthesized to tile the entire amino acid (aa) sequence of murine importin β 1, conjugated to N-terminal biotin, and screened in ELISA format on streptavidin-coated 96-well plates (supplemental Fig. S4A). This procedure led to the identification of a 20 aa epitope sequence corresponding to residues 301-320 of human KPNB1, within HEAT repeats

7 and 8. The alignment of the mouse, rat, human, and bovine importin β 1 protein sequence shows complete homology in the epitope region (Fig. 3A). We used PyMOL to visualize the identified epitope in the importin β 1 structure (49, 50), as shown in Figure 3B. To validate the affinity of the mAb for the identified sequence, we conducted reciprocal linear ELISAs, using either varying peptide dilutions (Fig. 3C) or varying mAb dilutions (Fig. 3D) and observed a linear signal increase until saturation. The mAb effectively recognizes Importin β 1 from different species in a number of applications, including ELISA, WB, IP (supplemental Fig. S4), and IF (supplemental Fig. S5). A direct comparison of the mAb performance in IF staining on several cell lines derived from different species is shown in supplemental Fig. S5.

To test the possibility of poor nuclear penetration of the antibody, 3T3 cells were treated with 0.1%, 1%, and 5% Triton. The cells were then simultaneously incubated with the mAb and rabbit anti-Nucleolin, which was used as a positive control for antibody recognition of nuclear proteins (51). The

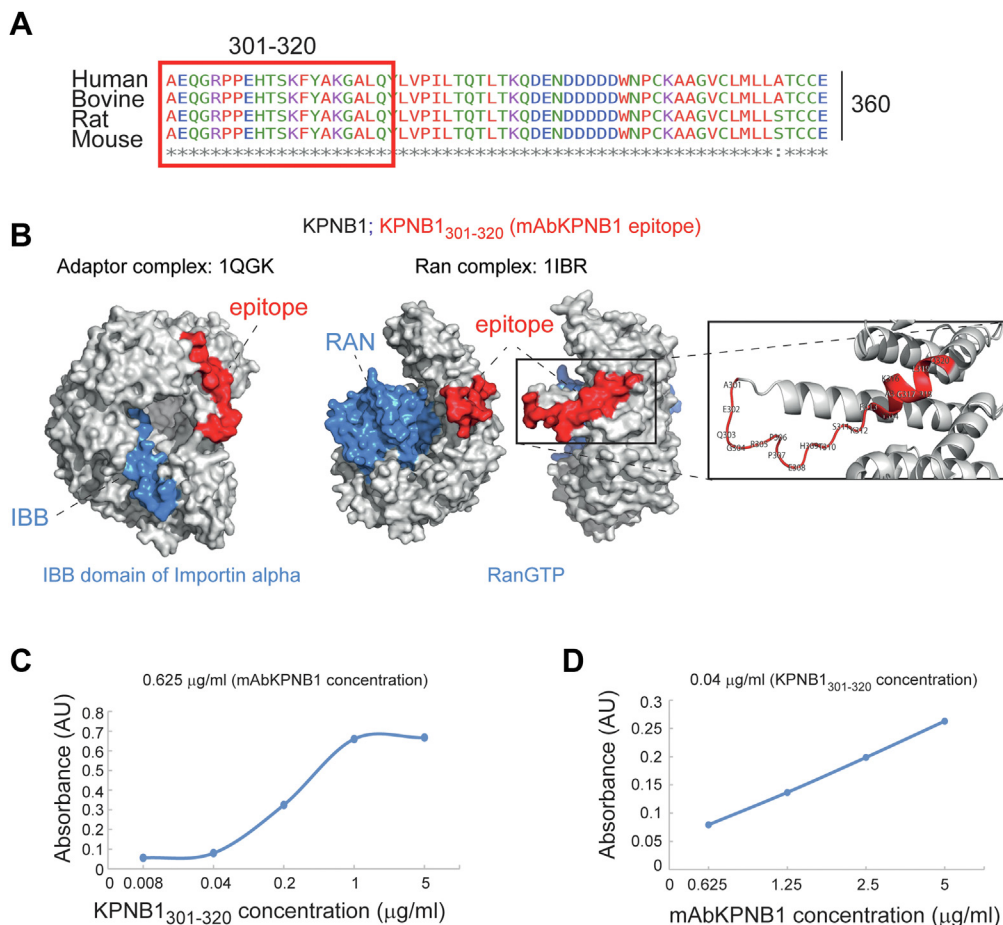


FIG. 3. **Epitope characterization of the mAb.** A, multiple sequence alignment shows homology of the identified epitope, comprising residues 301 to 320 of importin β 1, with color coding according to the physicochemical property of the amino acid by Clustal Omega. B, PyMOL generated representations of importin β 1 (gray) in complex with the N-terminal IBB domain of importin α (1QGK) or Ran (1IBR) (both in blue), with the identified epitope shown in red. Ran complex shown from two angles. C and D, ELISA data with serial dilutions of either peptide (C) or mAb (D) confirms dose-dependent recognition. IBB, Importin- β -binding domain.

results showed a clear nuclear localization of nucleolin immunoreactivity, but importin β 1 signal remained prominently cytoplasmic (supplemental Fig. S6). We also tested the effect of various fixatives and fixation times on mAbKPNB1-301-320 epitope recognition in HEK cells. The results showed that increasing the fixation time and adding 0.1% glutaraldehyde to 4% PFA reduced signal intensity but did not affect cytoplasmic preference in recognition of importin β 1 by the mAb (supplemental Fig. S7). We then verified whether the identified peptide epitope can serve as a blocking agent in IP assays. Preincubation of the mAb with the peptide prior to IP from rat brain lysates showed that KPNB1₃₀₁₋₃₂₀ competes with binding of endogenous full-length importin β 1, as demonstrated by reduced signal in the IP and no evident depletion in the supernatants (supplemental Fig. S8). Based on the validated epitope identity, the antibody is henceforth termed mAbKPNB1-301-320.

mAbKPNB1-301-320 Efficiently Recognizes Importin β 1 in Sensory Neurons

Locally translated importin β 1 is retrogradely transported from axon to soma in injured sensory neurons and is also associated with dynein in growing axons (20–22). We set out to test mAbKPNB1-301-320 in recognition of importin β 1 in sensory axons. Indeed, immunostaining of cultured neurons revealed strong cytoplasmic staining, which was absent in cells incubated in parallel with a blocking peptide comprising the epitope sequence (Fig. 4, A and B). Specific recognition of cytoplasmic and axonal importin- β 1 by mAbKPNB1-301-320 was also confirmed by immunogold labeling in electron microscopy sections of cultured sensory neurons (Fig. 4C) and by *in situ* PLA (supplemental Fig. S9, A and C). The latter method allows the detection of two epitopes, either on the same protein or on two interacting proteins, within a radius of 40 nm (52). Here, we used mAbKPNB1-301-320 together with a commercially available polyclonal anti-KPNB1 to detect importin- β 1 in the axons of cultured DRG neurons. Furthermore, we used PLA to validate the ability of mAbKPNB1-301-320 to recognize importin β 1 in association with dynein, robustly detecting colocalization of importin β 1 and dynein heavy chain (Dync1h1) in the axons of growing DRG neurons (Fig. 4, D and E).

In order to test the ability of mAbKPNB1-301-320 to detect axonal importin β 1 upregulation *in vivo*, we used the mouse model of SN crush injury. Nerves were isolated six hours after crush, fixed, and processed for immunohistochemistry for frozen sections. mAbKPNB1-301-320 detected significant upregulation of importin β 1 protein in injured SN axons (Fig. 5, A and B). Local upregulation of importin β 1 in axons after SN crush was also detected when using mAbKPNB1-301-320 for immunohistochemistry on paraffin sections (supplemental Fig. S10, A and B). Furthermore, we used PLA to validate the ability of mAbKPNB1-301-320 to detect importin β 1 in association with dynein in the SN. PLA signal significantly

increased after injury, confirming local translation of importin β 1 protein upon nerve injury and its binding to dynein for retrograde transport (Fig. 5, C–E). Little or no background was detected in both injured and noninjured PLA probe and antibody controls (supplemental Fig. S11).

mAbKPNB1-301-320 for BAR Analyses of Importin β 1 Cytoplasmic Interactomes

After thorough validation of mAbKPNB1-301-320, we tested its utility in capturing importin β 1 interactors using the BAR method on HEK cells (supplemental Fig. S12). A total of 276 importin β 1 proximal proteins were identified in this analysis (supplemental Fig. S12). Candidate proteins include nucleocytoplasmic transport proteins and strictly cytoplasmic interactors, such as the translation initiation factor EIF4B and the stress granule protein G3BP1 (supplemental Fig. S12, C and D and supplemental Table S3). Comparison of this dataset to a previously published BioID dataset for KPNB1 in HEK cells (17) revealed approximately 80% novel candidates, with a bias for cytoplasmic components, as compared to more nucleoplasmic representation in the BioID dataset (supplemental Fig. S12B). We then proceeded to use mAbKPNB1-301-320 for BAR analyses on DRG neurons grown for 3 days in culture. Streptavidin staining confirmed that biotinylation occurred in cytoplasm with negligible background signal from the nucleus (Fig. 6A). A total of 432 specific candidates were identified in this experiment (Fig. 6B and supplemental Table S4). String database analysis revealed that ~28% of these proteins are annotated as of neuron projection origin and ~18% as axonal proteins. Overall, 93% of the candidates were annotated as cytoplasmic proteins, some of these in overlap with hits annotated as occurring also in the nucleus. This overlap is not surprising for a nucleocytoplasmic transport protein. A number of functionally distinct complexes were identified, including components of the axonal growth cone, the dynein retrograde motor complex, axonal-dendritic transport proteins, Rho GTPase signaling systems, and markers for the cellular leading edge (Fig. 6, C and D, and supplemental Fig. S13). We also identified known importin β 1 cargos such as ribosomal proteins, STAT3, and vimentin, supplemental Table S4 (6, 7, 53). These results confirm mAbKPNB1-301-320 as a high-quality probe for importin β 1 interactomes.

DISCUSSION

In this study, we generated and validated a new mAb for importin β 1 and demonstrated its utility in proximity biotinylation analyses of importin β 1 interactomes using the BAR method. We turned to the BAR approach after initial attempts to use importin β 1/BirA* fusions for BioID, which identified various nuclear and nucleocytoplasmic transport interactors but revealed poor efficiency for identifying cytoplasmic interactors of the importins complex. The chemistry on which the

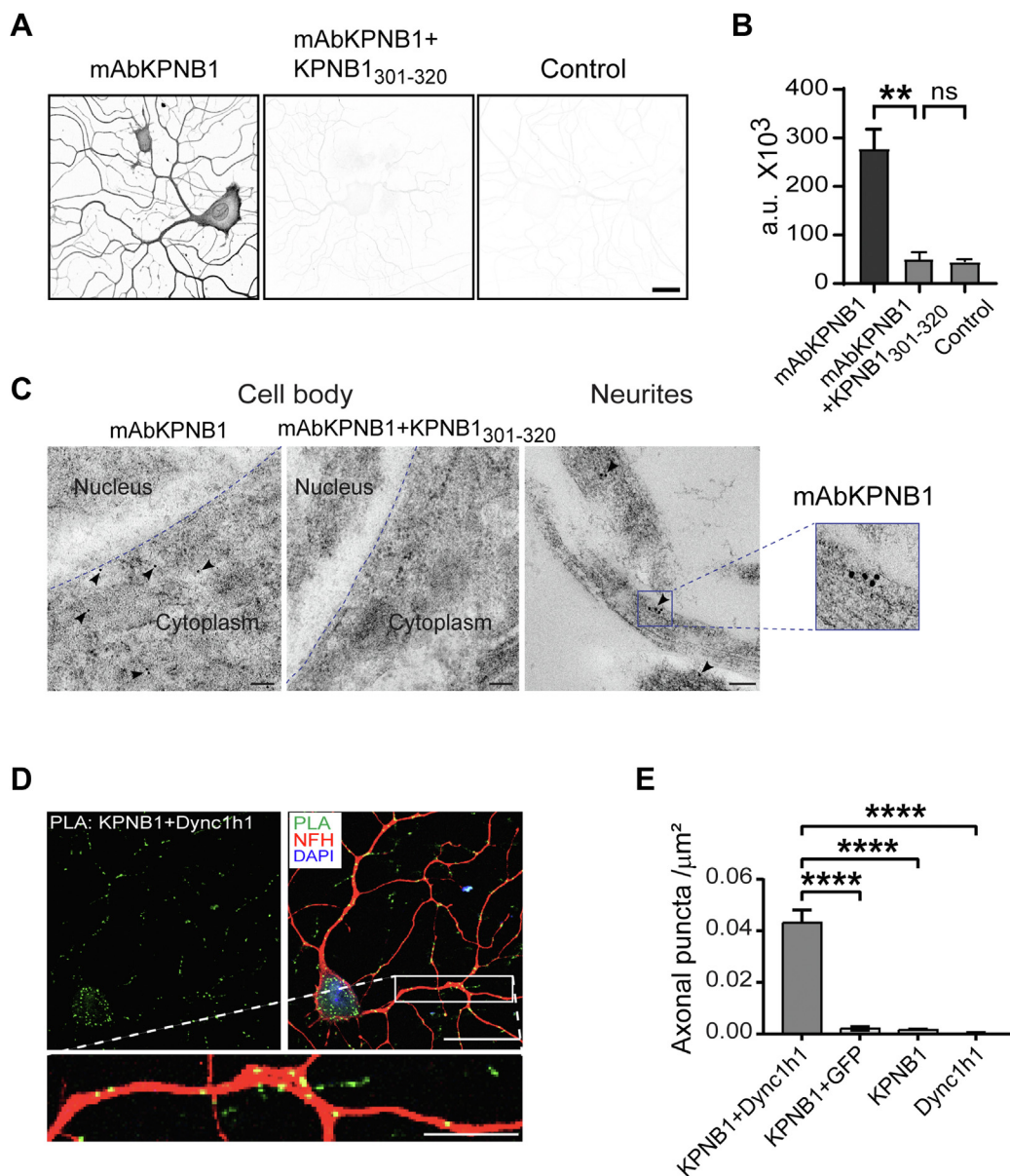


FIG. 4. mAbKPNB1-301-320 recognizes importin β 1 in adult DRG neurons. *A*, confocal images of adult DRG neurons in culture, stained for importin β 1 using mAbKPNB1-301-320 (mAbKPNB1, 4.6 nM). *Middle panel* after preincubation with a peptide comprising the epitope sequence (9.5 nM KPNB1₃₀₁₋₃₂₀), *right panel* is omitted primary antibody control. The scale bar represents 20 μ m. *B*, quantification of mAbKPNB1-301-320 average fluorescence intensity using ImageJ, Mean \pm SEM, $n \geq 5$, one-way ANOVA, ** indicates $p < 0.01$. *C*, electron micrographs of ultrathin monolayer sections showing immunogold labeling of importin β 1 in cultured mouse DRG neurons using mAbKPNB1-301-320 (mAbKPNB1, 0.1 μ g/ μ l), *left and right panels*. *Middle panel* after preincubation with a peptide comprising the epitope sequence (1 μ g/ μ l KPNB1₃₀₁₋₃₂₀). The scale bars represent 100 nm; gold particle diameter: 10 nm. *D*, proximity ligation assay (PLA, *green*) showing complexes of importin β 1 (KPNB1) with dynein (Dync1h1) in axons of cultured DRG neurons. Neurofilament heavy chain (NFH, *red*) and DAPI (*blue*). Scale bars: full image 50 μ m, insert 10 μ m. *E*, quantification of PLA signal in axons, one-way ANOVA with Dunnett's multiple comparisons test, **** indicates $p < 0.0001$, $n > 13$. DRG, dorsal root ganglia.

BAR method is based has a significantly larger labeling range than BioID (26, 48), and the method does not require the introduction of exogenous tags to the protein of interest. These characteristics are advantageous for comprehensive coverage of interactomes of interest, but conversely, they may

decrease the specificity of the analysis. Hence, the effective use of BAR is critically dependent on the antibody quality. mAbKPNB1-301-320 was shown to be a highly specific and sensitive importin β 1 probe in a broad range of applications, cell types, and species. Mapping localized the epitope to

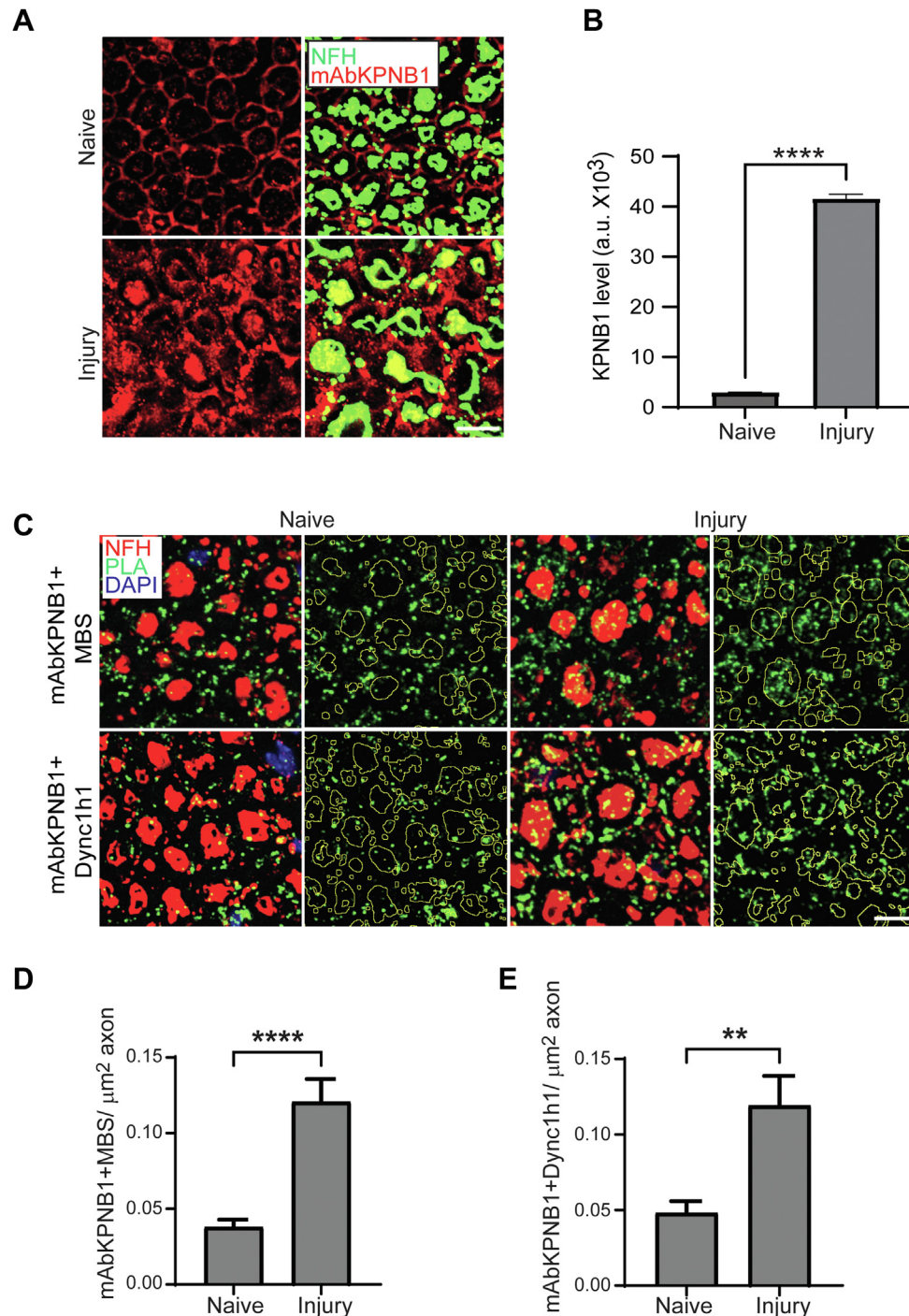


FIG. 5. mAbKPNB1-301-320 detects importin β 1 upregulation in injured nerve. *A*, immunostaining of cryosections with mAbKPNB1-301-320 (mAbKPNB1, 2.7 ng/ μ l) before and 24 h after sciatic nerve crush. The scale bar represents 10 μ m. *B*, quantification of analysis shown in (*A*) in ImageJ, using NFH staining as a mask for axons. Mean \pm SEM, $n \geq 490$ axons, Unpaired two-tailed *t* test, **** indicates $p < 0.0001$. *C*, confocal imaging of PLA. *Upper*, PLA for importin β 1 with mAbKPNB1 and a commercial anti-KPNB1 antibody (MBS); *lower*: PLA for dynein and importin β 1 with anti-Dync1h1 and mAbKPNB1; both on cross sections of the sciatic nerve, the scale bar represents 5 μ m. *D* and *E*, Quantification of the analyses shown in (*C*), for importin β 1 specific detection (*D*) or importin β 1 in complex with dynein (*E*). Mean \pm SEM, $n > 2000$ axons, Unpaired two-tailed *t* test, ** indicates $p < 0.01$, **** $p < 0.0001$.

amino acids 301 to 320 in importin β 1, and importantly, the linear 20-mer peptide epitope is effective as a blocking reagent in different assays. Visualization of the epitope in the

importin β 1 crystal structure localizes it to a concave feature within the stalk motif that does not overlap with Ran-binding sites (Fig. 3B) (50). The epitope protrudes by ~ 20 \AA from the

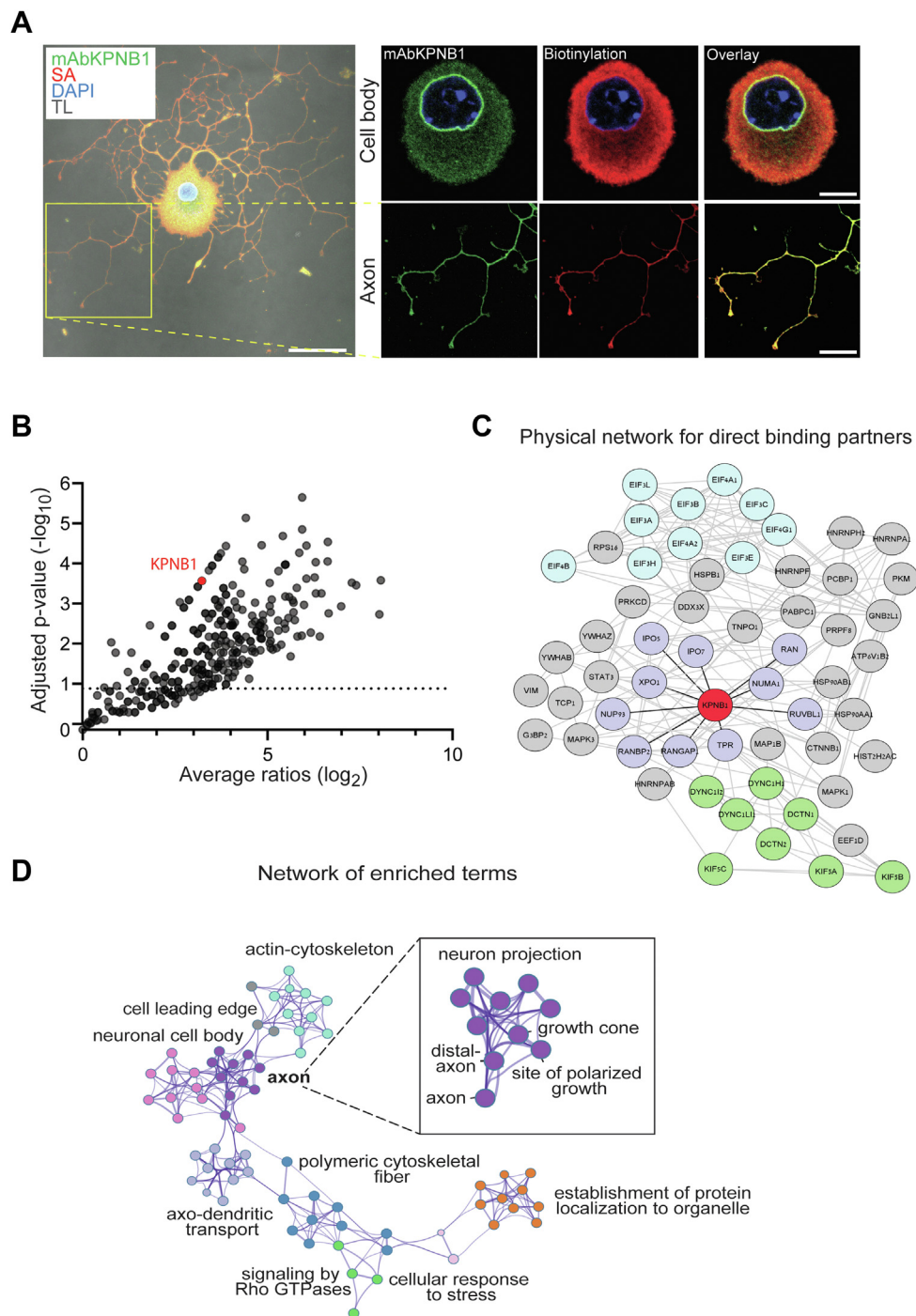


FIG. 6. BAR characterization of the cytoplasmic importin β 1 interactome in adult DRG neurons. *A*, visualization of mAbKPNB1-301-320-directed BAR reaction in a cultured DRG neuron, showing endogenous cytoplasmic importin β 1 (green) and biotinylation (red). Scale bars: full image 40 μ m, cell body 10 μ m, axon 20 μ m. Note the predominantly cytoplasmic and axonal biotinylation. *B*, volcano plot of proteins identified by mass spectrometry with BAR, multiple *t* test with a desired false discovery rate of 10%, *n* = 3. *C*, network analysis of hits from (*B*) showing subnetwork of direct binding partners based on STRING database. KPNB1 in red, retrograde motor interactors in green, translation machinery in light blue, nucleocytoplasmic transport in light purple, and other second order interactors in gray. *D*, partial network of selected enriched terms with focus on the axonal compartment: colored by cluster ID, nodes that share the same cluster ID are closer to each other, generated by Metascape. BAR, biotinylation by antibody recognition; DRG, dorsal root ganglia.

surface of the protein and is clearly accessible to the antibody in cytoplasmic and axonal compartments, but less available within nuclei. Specific functions of the stalk motif are unknown, and the subcellular specificity of our new mAb might suggest a difference in occupancy of this region between nucleus and cytoplasm. The significance of this subcellular specificity for importin β 1 functions will be an intriguing topic for future exploration, and the antibody provides an excellent tool for this purpose.

Previous characterizations of importin β 1 interactomes used a diversity of approaches, including BioID (17), SILAC-Tp (12, 54, 55), and co-IP methods (18, 19). Different cell types and biological paradigms were used in these studies, complicating direct comparison of those datasets with ours. However, gene ontology analyses allow more comprehensive comparisons, and these are shown for subcellular localization and canonical pathway analyses in Figure 7. Unsurprisingly, both BAR datasets from the present study showed a higher representation of cytoplasmic proteins than the previous datasets, reflecting the subcellular preference of the antibody. This subcellular specificity is also reflected in the signaling pathways identified by BAR versus previous BioID and pull-down approaches (Fig. 7A), highlighting the need for diverse approaches in multiple cell types for truly comprehensive profiling of such interactomes. It should however be noted that the BioID studies conducted with KPNB1 to date have all used first or second generation BirA* enzymes, and it is possible that enhanced activity or faster

acting variants developed recently (24, 56) would be more efficient.

In summary, we have generated an antibody that discriminates between subcellular conformations of importin β 1 and have shown that it provides a highly specific and sensitive probe for cytoplasmic importin complexes. BAR analyses utilizing the new antibody as a targeting agent reveal significant new categories of the importin β 1 interactome, with focus on cytoplasmic and signaling proteins that highlight new functional roles of the importins complex that go beyond nucleocytoplasmic transport.

DATA AVAILABILITY

The mass spectrometry proteomics data have been deposited to the ProteomeXchange Consortium via the PRIDE (57) partner repository with the dataset identifier PXD032728. The mAbKPNB1-301-320 antibody will be available through the Ximbio repository (<https://ximbio.com/>). Data are available via ProteomeXchange with identifier PXD032728.

Supplemental data—This article contains [supplemental data](#) (30–32).

Acknowledgments—We sincerely thank Prof. Zelig Eshhar and Tova Waks for their advice on monoclonal antibody generation; Vladimir Kiss for assistance with microscopy; Dr. Reinat Nevo for software expertise on image analysis; Dr. Vera

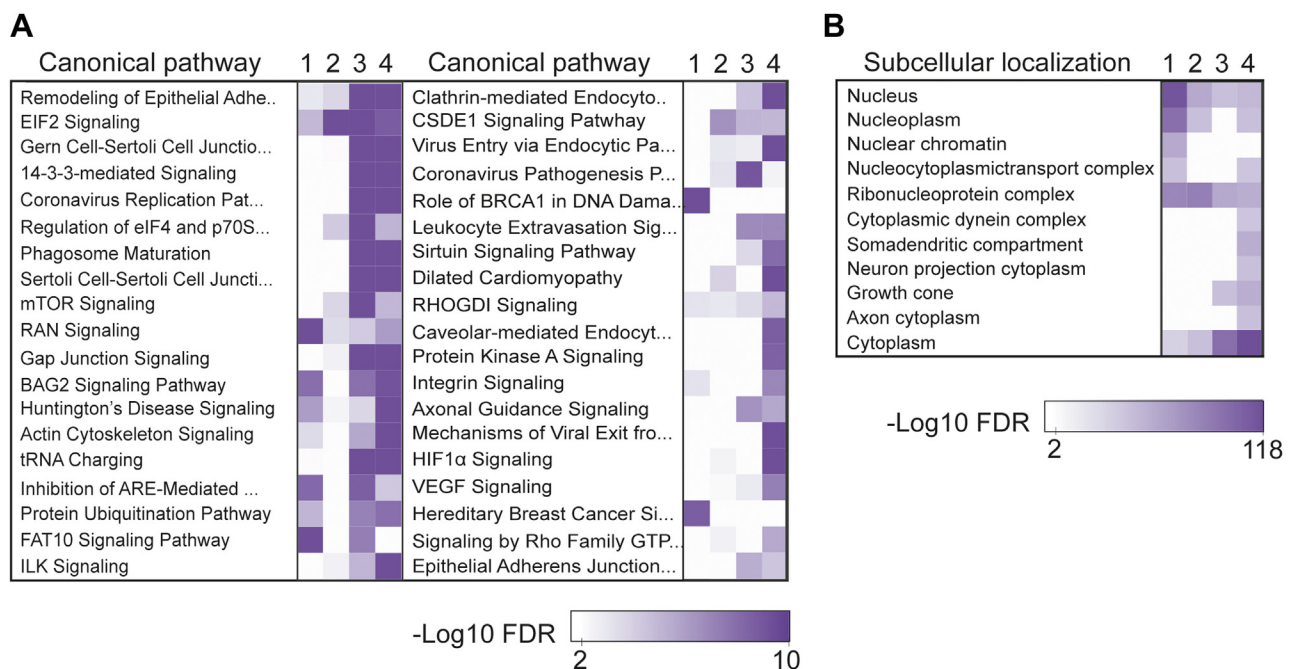


FIG. 7. **Gene ontology comparisons of different importin β 1 interactomes.** Gene ontology analyses from datasets of (1) Reference #17 (HEK293T), (2) References #18, #19 (HeLa), (3) HEK 293T BAR, and (4) DRG neuron BAR. *A*, canonical pathway comparison using Ingenuity pathway analysis sorted by score value and a 1% p value cut-off. *B*, GO analysis using STRING categories for subcellular localization, p value cut-off: 1%. BAR, biotinylation by antibody recognition; DRG, dorsal root ganglia; HEK, human embryonic kidney.

Shinder and Dr. Eyal Shimoni for assistance with electron microscopy; and Dr. Dalia Gordon for helpful discussions. Electron microscopy studies were conducted at the Irving and Cherna Moskowitz Center for Nano and Bio-Nano Imaging at the Weizmann Institute of Science.

Funding and additional information—We gratefully acknowledge funding from the Israel Science Foundation (ISF 1337/18 to M. F. & I. R.), and the Dr. Miriam and Sheldon G. Adelson Medical Research Foundation (to A. L. B. & M. F.). C. A. A. was supported by a long-term fellowship from the Human Frontier Science Program Organization. M. F. is the incumbent of the Chaya Professorial Chair in Molecular Neuroscience at the Weizmann Institute of Science.

Author contributions—D.-A. S., S. A., E. D.-M., C. A. A., M. F., and I. R. methodology; D.-A. S., S. A., E. D.-M., V. S., C. A. A., O. L., H. H., J. A. O.-P., N. D., and I. R. investigation; D.-A. S., S. A., E. D.-M., V. S., C. A. A., O. L., H. H., N. D., and I. R. formal analysis; A. L. B., M. F., and I. R. supervision; D.-A. S., S. A., E. D.-M., M. F., and I. R. writing—original draft; D.-A. S., S. A., E. D.-M., V. S., C. A. A., O. L., H. H., J. A. O.-P., N. D., A. L. B., M. F., and I. R. writing—review and editing.

Conflicts of interest—The authors declare that they have no conflicts of interest with the contents of this article.

Abbreviations—The abbreviations used are: BAR, biotinylation by antibody recognition; BSA, bovine serum albumin; CFA, Complete Freund's Adjuvant; DRG, dorsal root ganglia; FBS, fetal bovine serum; HEK, human embryonic kidney; IBB, importin- β -binding domain; IF, immunofluorescence; IP, immunoprecipitation; NLS, nuclear localization signal; PBST, PBS containing 0.05% Tween-20; PLA, proximity ligation assay; PSM, Peptide Spectral Match; SN, sciatic nerve; TB, transport buffer; WB, Western blot; WES, Western capillary system.

Received March 25, 2022, and in revised form, September 20, 2022
Published, MCPRO Papers in Press, September 28, 2022, <https://doi.org/10.1016/j.mcpro.2022.100418>

REFERENCES

- Chang, C.-C., and Hsia, K.-C. (2021) More than a zip code: global modulation of cellular function by nuclear localization signals. *FEBS J.* **288**, 5569–5585
- Kalita, J., Kapinos, L. E., and Lim, R. Y. H. (2021) On the asymmetric partitioning of nucleocytoplasmic transport – recent insights and open questions. *J. Cell Sci.* **134**, jcs240382
- Rishal, I., and Fainzilber, M. (2019) Cell size sensing - a one-dimensional solution for a three-dimensional problem? *BMC Biol.* **17**, 36
- Terenzio, M., Schiavo, G., and Fainzilber, M. (2017) Compartmentalized signaling in neurons: from cell biology to neuroscience. *Neuron* **96**, 667–679
- Nguyen, T., Pappireddi, N., and Wuhr, M. (2019) Proteomics of nucleocytoplasmic partitioning. *Curr. Opin. Chem. Biol.* **48**, 55–63
- Perlson, E., Hanz, S., Ben-Yaakov, K., Segal-Ruder, Y., Seger, R., and Fainzilber, M. (2005) Vimentin-dependent spatial translocation of an activated MAP kinase in injured nerve. *Neuron* **45**, 715–726
- Ben-Yaakov, K., Dagan, S. Y., Segal-Ruder, Y., Shalem, O., Vuppalachchi, D., Willis, D. E., et al. (2012) Axonal transcription factors signal retrogradely in lesioned peripheral nerve. *EMBO J.* **31**, 1350–1363
- Karpova, A., Mikhaylova, M., Bera, S., Bar, J., Reddy, P. P., Behnisch, T., et al. (2013) Encoding and transducing the synaptic or extrasynaptic origin of NMDA receptor signals to the nucleus. *Cell* **152**, 1119–1133
- Lieu, K. G., Shim, E. H., Wang, J., Lokareddy, R. K., Tao, T., Cingolani, G., et al. (2014) The p53-induced factor Ei24 inhibits nuclear import through an importin beta-binding-like domain. *J. Cell Biol.* **205**, 301–312
- Al-Wassiti, H. A., Thomas, D. R., Wagstaff, K. M., Fabb, S. A., Jans, D. A., Johnston, A. P., et al. (2021) Adenovirus terminal protein contains a bipartite nuclear localisation signal essential for its import into the nucleus. *Int. J. Mol. Sci.* **22**, 3310
- Michaevskii, I., Segal-Ruder, Y., Rozenbaum, M., Medzihradsky, K. F., Shalem, O., Coppola, G., et al. (2010) Signaling to transcription networks in the neuronal retrograde injury response. *Sci. Signal.* **3**, ra53
- Kimura, M., Morinaka, Y., Imai, K., Kose, S., Horton, P., and Imamoto, N. (2017) Extensive cargo identification reveals distinct biological roles of the 12 importin pathways. *ELife* **6**, e21184
- Yasuhara, N., Yamagishi, R., Arai, Y., Mehmood, R., Kimoto, C., Fujita, T., et al. (2013) Importin alpha subtypes determine differential transcription factor localization in embryonic stem cells maintenance. *Dev. Cell* **26**, 123–135
- Hugel, S., Depping, R., Dittmar, G., Rother, F., Cabot, R., Sury, M. D., et al. (2014) Identification of importin alpha 7 specific transport cargoes using a proteomic screening approach. *Mol. Cell. Proteomics* **13**, 1286–1298
- Panayotis, N., Sheinin, A., Dagan, S. Y., Tsoory, M. M., Rother, F., Vadhvani, M., et al. (2018) Importin alpha5 regulates anxiety through MeCP2 and sphingosine kinase 1. *Cell Rep.* **25**, 3169–3179
- Marvaldi, L., Panayotis, N., Alber, S., Dagan, S. Y., Okladnikov, N., Koppel, I., et al. (2020) Importin alpha3 regulates chronic pain pathways in peripheral sensory neurons. *Science* **369**, 842–846
- Mackmull, M. T., Klaus, B., Heinze, I., Chokkalingam, M., Beyer, A., Russell, R. B., et al. (2017) Landscape of nuclear transport receptor cargo specificity. *Mol. Syst. Biol.* **13**, 962
- Verrico, A., Rovella, P., Di Francesco, L., Damizia, M., Staid, D. S., Le Pera, L., et al. (2020) Importin-beta/karyopherin-beta1 modulates mitotic microtubule function and taxane sensitivity in cancer cells via its nucleoporin-binding region. *Oncogene* **39**, 454–468
- Di Francesco, L., Verrico, A., Asteriti, I. A., Rovella, P., Cirigliano, P., Guarguaglini, G., et al. (2018) Visualization of human karyopherin beta-1/importin beta-1 interactions with protein partners in mitotic cells by co-immunoprecipitation and proximity ligation assays. *Sci. Rep.* **8**, 1850
- Hanz, S., Perlson, E., Willis, D., Zheng, J.-Q., Massarwa, R.a., Huerta, J. J., et al. (2003) Axoplasmic importins enable retrograde injury signaling in lesioned nerve. *Neuron* **40**, 1095–1104
- Perry, R. B., Doron-Mandel, E., Iavnilovitch, E., Rishal, I., Dagan, S. Y., Tsoory, M., et al. (2012) Subcellular knockout of importin beta1 perturbs axonal retrograde signaling. *Neuron* **75**, 294–305
- Perry, R. B., Rishal, I., Doron-Mandel, E., Kalinski, A. L., Medzihradsky, K. F., Terenzio, M., et al. (2016) Nucleolin-mediated RNA localization regulates neuron growth and cycling cell size. *Cell Rep.* **16**, 1664–1676
- Terenzio, M., Koley, S., Samra, N., Rishal, I., Zhao, Q., Sahoo, P. K., et al. (2018) Locally translated mTOR controls axonal local translation in nerve injury. *Science* **359**, 1416–1421
- Samavarchi-Tehrani, P., Samson, R., and Gingras, A. C. (2020) Proximity dependent biotinylation: key enzymes and adaptation to proteomics approaches. *Mol. Cell. Proteomics* **19**, 757–773
- Roux, K. J., Kim, D. I., Raida, M., and Burke, B. (2012) A promiscuous biotin ligase fusion protein identifies proximal and interacting proteins in mammalian cells. *J. Cell Biol.* **196**, 801–810
- Bar, D. Z., Atkatsch, K., Tavarez, U., Erdos, M. R., Gruenbaum, Y., and Collins, F. S. (2018) Biotinylation by antibody recognition—a method for proximity labeling. *Nat. Methods* **15**, 127–133
- Bar, D. Z., Atkatsch, K., Tavarez, U., Erdos, M. R., Gruenbaum, Y., and Collins, F. S. (2018) Addendum: biotinylation by antibody recognition—a method for proximity labeling. *Nat. Methods* **15**, 749

28. Bobrow, M. N., Harris, T. D., Shaughnessy, K. J., and Litt, G. J. (1989) Catalyzed reporter deposition, a novel method of signal amplification. Application to immunoassays. *J. Immunol. Methods* **125**, 279–285
29. van Gijlswijk, R. P., Zijlmans, H. J., Wiegant, J., Bobrow, M. N., Erickson, T. J., Adler, K. E., et al. (1997) Fluorochrome-labeled tyramides: use in immunocytochemistry and fluorescence *in situ* hybridization. *J. Histochem. Cytochem.* **45**, 375–382
30. Peleg, Y., and Unger, T. (2014) Application of the restriction-free (RF) cloning for multicomponents assembly. *Methods Mol. Biol.* **1116**, 73–87
31. Unger, T., Jacobovitch, Y., Dantes, A., Bernheim, R., and Peleg, Y. (2010) Applications of the restriction free (RF) cloning procedure for molecular manipulations and protein expression. *J. Struct. Biol.* **172**, 34–44
32. Eshhar, Z. (1985) Monoclonal antibody strategy and techniques. In: Springer, T. A., ed. *Hybridoma Technology in the Biosciences and Medicine*, Springer US, Boston, MA: 3–41
33. Rishal, I., Kam, N., Perry, R. B., Shinder, V., Fisher, E. M., Schiavo, G., et al. (2012) A motor-driven mechanism for cell-length sensing. *Cell Rep.* **1**, 608–616
34. Doron-Mandel, E., Alber, S., Oses, J. A., Medzihradsky, K. F., Burlingame, A. L., Fainzilber, M., et al. (2016) Isolation and analyses of axonal ribonucleoprotein complexes. *Methods Cell Biol.* **131**, 467–486
35. Harris, V. M. (2015) Protein detection by simple western analysis. *Methods Mol. Biol.* **1312**, 465–468
36. Schindelin, J., Arganda-Carreras, I., Frise, E., Kaynig, V., Longair, M., Pietzsch, T., et al. (2012) Fiji: an open-source platform for biological-image analysis. *Nat. Methods* **9**, 676–682
37. Roux, K. J., Kim, D. I., and Burke, B. (2013) BioID: a screen for protein-protein interactions. *Curr. Protoc. Protein Sci.* **74**, 19 23 11–19 23 14
38. Guan, S., Price, J. C., Prusiner, S. B., Ghaemmaghami, S., and Burlingame, A. L. (2011) A data processing pipeline for mammalian proteome dynamics studies using stable isotope metabolic labeling. *Mol. Cell. Proteomics* **10**, M111 010728
39. Clauser, K. R., Baker, P., and Burlingame, A. L. (1999) Role of accurate mass measurement (\pm 10 ppm) in protein identification strategies employing MS or MS/MS and database searching. *Anal. Chem.* **71**, 2871–2882
40. Benjamini, Y., Krieger, A. M., and Yekutieli, D. (2006) Adaptive linear step-up procedures that control the false discovery rate. *Biometrika* **93**, 491–507
41. Szklarczyk, D., Gable, A. L., Nastou, K. C., Lyon, D., Kirsch, R., Pyysalo, S., et al. (2021) The STRING database in 2021: customizable protein-protein networks, and functional characterization of user-uploaded gene/measurement sets. *Nucleic Acids Res.* **49**, D605–D612
42. Zhou, Y., Zhou, B., Pache, L., Chang, M., Khodabakhshi, A. H., Tanaseichuk, O., et al. (2019) Metascape provides a biologist-oriented resource for the analysis of systems-level datasets. *Nat. Commun.* **10**, 1523
43. Kim, D. I., Birendra, K. C., Zhu, W., Motamedchaboki, K., Doye, V., and Roux, K. J. (2014) Probing nuclear pore complex architecture with proximity-dependent biotinylation. *Proc. Natl. Acad. Sci. U. S. A.* **111**, E2453–E2461
44. Lott, K., and Cingolani, G. (2011) The importin beta binding domain as a master regulator of nucleocytoplasmic transport. *Biochim. Biophys. Acta* **1813**, 1578–1592
45. Herold, A., Truant, R., Wiegand, H., and Cullen, B. R. (1998) Determination of the functional domain organization of the importin alpha nuclear import factor. *J. Cell Biol.* **143**, 309–318
46. Miyamoto, Y., Yamada, K., and Yoneda, Y. (2016) Importin alpha: a key molecule in nuclear transport and non-transport functions. *J. Biochem.* **160**, 69–75
47. Carter, D., Chakalova, L., Osborne, C. S., Dai, Y. F., and Fraser, P. (2002) Long-range chromatin regulatory interactions *in vivo*. *Nat. Genet.* **32**, 623–626
48. Chen, Y., Zhang, Y., Wang, Y., Zhang, L., Brinkman, E. K., Adam, S. A., et al. (2018) Mapping 3D genome organization relative to nuclear compartments using TSA-Seq as a cytological ruler. *J. Cell Biol.* **217**, 4025–4048
49. Cingolani, G., Petosa, C., Weis, K., and Muller, C. W. (1999) Structure of importin-beta bound to the IBB domain of importin-alpha. *Nature* **399**, 221–229
50. Vetter, I. R., Arndt, A., Kutay, U., Gorlich, D., and Wittinghofer, A. (1999) Structural view of the Ran-importin beta interaction at 2.3 Å resolution. *Cell* **97**, 635–646
51. Doron-Mandel, E., Koppel, I., Abraham, O., Rishal, I., Smith, T. P., Buchanan, C. N., et al. (2021) The glycine arginine-rich domain of the RNA-binding protein nucleolin regulates its subcellular localization. *EMBO J.* **40**, e107158
52. Soderberg, O., Gullberg, M., Jarvius, M., Ridderstrale, K., Leuchowius, K. J., Jarvius, J., et al. (2006) Direct observation of individual endogenous protein complexes *in situ* by proximity ligation. *Nat. Methods* **3**, 995–1000
53. Luo, Y., Wang, Z., Tian, L., and Li, X. (2013) The function of importin beta1 is conserved in eukaryotes but the substrates may vary in organisms. *Plant Signal. Behav.* **8**, e25106
54. Kimura, M., Okumura, N., Kose, S., Takao, T., and Imamoto, N. (2013) Identification of cargo proteins specific for importin-beta with importin-alpha applying a stable isotope labeling by amino acids in cell culture (SILAC)-based *in vitro* transport system. *J. Biol. Chem.* **288**, 24540–24549
55. Kimura, M., Thakar, K., Karaca, S., Imamoto, N., and Kehlenbach, R. H. (2014) Novel approaches for the identification of nuclear transport receptor substrates. *Methods Cell Biol.* **122**, 353–378
56. Zhou, Y., and Zou, P. (2021) The evolving capabilities of enzyme-mediated proximity labeling. *Curr. Opin. Chem. Biol.* **60**, 30–38
57. Perez-Riverol, Y., Bai, J., Bandla, C., Garcia-Seisdedos, D., Hewapathirana, S., Kamatchinathan, S., et al. (2022) The PRIDE database resources in 2022: a hub for mass spectrometry-based proteomics evidences. *Nucleic Acids Res.* **50**, D543–D552